Kinetics of ordering and spinodal decomposition in the pair approximation

Long-Qing Chen
Department of Materials Science and Engineering, The Pennsylvania State University, University Park, Pennsylvania 16802
(Received 15 January 1998)

The kinetics of atomic ordering and phase separation in inhomogeneous systems were investigated employing microscopic master equations in the pair approximation. For a homogeneous system at completely thermodynamic equilibrium, the kinetic equations produce the same equilibrium states as the cluster variation method. We studied the kinetics of both short- and long-range order and spinodal decomposition kinetics, as well as the morphological pattern formation and evolution. It is shown that the development of long-range order and growth of concentration wave amplitudes are significantly delayed due to the decreases in driving forces as a result of short-range order relaxation in the pair approximation as compared to that obtained from the point approximation with the same initial condition. It is demonstrated that the kinetics obtained by assuming the pair distribution functions always at equilibrium is found to be a good approximation for the pair approximation. The effect of bond energies on the ordering kinetics will be discussed.
[S0163-1829(98)08033-3]

INTRODUCTION

Recently, the continuum Cahn-Hilliard and Allen-Cahn equations[1,2] and their microscopic counterparts, the Khachaturyan microscopic diffusion equations,[3] have been extensively employed to study the kinetics of atomic ordering, compositional phase separation, and particularly, domain coarsening.[4–6] They have been very successful in predicting the sequence of phase transformations as well as the kinetics of domain coarsening. All these equations are based on a free-energy functional that depends on a local order parameter or the local composition in the continuum model or the point probabilities in the microscopic model. They describe the rate change of order parameters or occupation probabilities with respect to time as *linearly* proportional to the thermodynamic driving force. Therefore, in principle, the quantitative description of kinetics by these models is only valid when a system is not too far from equilibrium, i.e., the driving force for a given diffusional process is small, e.g., during domain coarsening.

In other types of kinetic models, including the microscopic master equations[7–15] and the path probability method (PPM) (Refs. 16–22), free-energy functionals do not explicitly enter into the kinetic equations of motion. In principle, high-order atomic correlations such as pair and tetrahedral correlations can be taken into account. The rate of change of an order parameter is highly nonlinear with respect to the thermodynamic driving force, so they are valid for systems with a high degree of nonequilibrium. The dependency of atomic diffusion or exchange on the local atomic configuration is automatically considered. However, essentially all early applications of PPM and microscopic master equations assumed transitional symmetry and were concerned with homogeneous systems. They were almost exclusively devoted to order-disorder transformations in homogeneous systems as is necessitated in that context.

Very recently, there have been a number of applications of the microscopic master equation approach to inhomogeneous systems. For example, van Baal investigated the kinetics of ordering and spinodal decomposition in one-dimensional inhomogeneous systems using the microscopic master equations with the nearest-neighbor pair approximation.[23] We applied the microscopic master equations to ordering and phase separation processes in two-dimensional inhomogeneous systems with or without surfaces using a second-neighbor interaction model in both point and pair approximations.[24–27] More recently, similar microscopic kinetic master equations based on the single-site approximation were applied to ordering and phase separation kinetics in two-dimensional inhomogeneous alloys by Vaks, Beiden, and Dobretsov[28–30] and Plapp and Gouyet.[31,32]

It is well known that the pair approximation yields more accurate results than the point approximation for the equilibrium thermodynamic properties for a two-dimensional square lattice, as well as a three-dimensional bcc lattice. The main purpose of this paper is to examine the differences in the kinetics of ordering and phase separation obtained from a point approximation and that from a pair approximation with the same set of interaction parameters. In particular, we will show that the incubation time for ordering and spinodal decomposition is significantly larger in the pair approximation than in the point approximation. However, we also showed that, although in the pair approximation the kinetics of long-range order is coupled with that of short-range order relaxation, it can be very well approximated by assuming that short-range order is instantaneously established, i.e., the short-range order is slaved by the long-range order.

THE KINETIC MODEL

For an A-B binary alloy in the pair approximation, the structural state at a given temperature is described by point and pair distribution functions denoted as $P_{\alpha}(\mathbf{r})$ and $P_{\alpha_1,\alpha_2}(\mathbf{r}_1,\mathbf{r}_2)$ where α and $\mathbf{r}$ represent the type of atom and lattice position,[7,24] respectively. These distribution functions satisfy the following normalization conditions:

$$\sum_{\alpha} P_{\alpha}(\mathbf{r})=1,$$

$$\sum_{\alpha_2} P_{\alpha_1,\alpha_2}(\mathbf{r}_1,\mathbf{r}_2)=P_{\alpha_1}(\mathbf{r}_1), \tag{1}$$

$$\sum_{\alpha_1} P_{\alpha_1,\alpha_2}(\mathbf{r}_1,\mathbf{r}_2)=P_{\alpha_2}(\mathbf{r}_2).$$

Therefore, they are not independent. Among them, we can choose an independent set, e.g., $P_A(\mathbf{r})$ and $P_{AA}(\mathbf{r}_1,\mathbf{r}_2)$. All other point and pair variables may be obtained from this independent set according to the normalization condition (1).

Away from equilibrium, all distribution functions will change with time as the atomic diffusion takes place in a system. Although both vacancy and direct exchange mechanisms can be treated in this formulation,[25,26] we shall assume a direct exchange mechanism in this work for simplicity.

Let us consider a pair of exchange sites at $\mathbf{r}$ and a nearest-neighbor site $\mathbf{r}+\delta$, and a set $\{\mathbf{x}\}$ of nearby influence sites that can affect the exchange reaction. If we have an A atom at $\mathbf{r}$, a B atom at $\mathbf{r}+\delta$, and a set of atoms $\{x\}$ at $\{\mathbf{x}\}$, we use $R_{AB}(\{\mathbf{x}\})$ to represent the rate at which the AB pair exchanges under the influence of the set of neighboring atoms $\{x\}$. Similarly, $R_{BA}(\{x\})$ is the rate at which a BA pair will exchange under the same environment when a B atom is at $\mathbf{r}$, and an A atom is at $\mathbf{r}+\delta$. Then the rates of change of $P_A(\mathbf{r})$ and $P_{AA}(\mathbf{r}_1,\mathbf{r}_2)$ are given by

$$\frac{dP_A(\mathbf{r})}{dt}=\sum_{\delta}\sum_{\{x\}} P_{BA\{x\}}(\mathbf{r},\mathbf{r}+\delta,\{\mathbf{x}\})R_{BA}(\{x\}) - \sum_{\delta}\sum_{\{x\}} P_{AB\{x\}}(\mathbf{r},\mathbf{r}+\delta,\{\mathbf{x}\})R_{AB}(\{x\}), \tag{2}$$

$$\begin{aligned}\frac{dP_{AA}(\mathbf{r}_1,\mathbf{r}_2)}{dt} &= \sum_{\delta\neq\mathbf{r}_1-\mathbf{r}_2}\sum_{\{x\}} P_{ABA\{x\}}(\mathbf{r}_1,\mathbf{r}_2,\mathbf{r}_2+\delta,\{\mathbf{x}\})R_{BA}(\{x\}) \\ &+ \sum_{\delta\neq\mathbf{r}_2-\mathbf{r}_1}\sum_{\{x\}} P_{BAA\{x\}}(\mathbf{r}_1,\mathbf{r}_2,\mathbf{r}_1+\delta,\{\mathbf{x}\})R_{BA}(\{x\}) \\ &- \sum_{\delta\neq\mathbf{r}_1-\mathbf{r}_2}\sum_{\{x\}} P_{AAB\{x\}}(\mathbf{r}_1,\mathbf{r}_2,\mathbf{r}_2+\delta,\{\mathbf{x}\})R_{AB}(\{x\}) \\ &- \sum_{\delta\neq\mathbf{r}_2-\mathbf{r}_1}\sum_{\{x\}} P_{AAB\{x\}}(\mathbf{r}_1,\mathbf{r}_2,\mathbf{r}_1+\delta,\{\mathbf{x}\})R_{AB}(\{x\}),\end{aligned} \tag{3}$$

where Σ_δ denotes the summation over all the nearest-neighbor sites $\mathbf{r}+\delta$ of $\mathbf{r}$. In Eqs. (2) and (3), $P_{\alpha_1,\alpha_2,\ldots,\alpha_n}(\mathbf{r}_1,\mathbf{r}_2,\ldots,\mathbf{r}_n)$ represents the joint probability of $\alpha_1,\alpha_2,\ldots,\alpha_n$ occupying $\mathbf{r}_1,\mathbf{r}_2,\ldots,\mathbf{r}_n$ simultaneously. For example, $P_{AB\{x\}}(\mathbf{r},\mathbf{r}+\delta,\{\mathbf{x}\})$ is the probability of simultaneously finding an A atom at $\mathbf{r}$, a B atom at $\mathbf{r}+\delta$, and the atomic species $X_1,\ldots,$ (in this case either an A atom or a B atom) of the set $\{x\}$ at the neighboring sites $x_1,\ldots,$ in the site set $\{\mathbf{x}\}$.

In order to carry out the summations in the right-hand side of Eqs. (2) and (3), we need to express the joint probability distributions, $P_{AB\{x\}}(\mathbf{r},\mathbf{r}+\delta,\{\mathbf{x}\})$, etc., in terms of independent point and pair distribution functions. For this purpose, we invoke the superposition approximation. In the pair approximation this takes the form

$$P_{\{x'\}}(\{\mathbf{x}'\})=\prod_{x_i\in\{\mathbf{x}'\}} P_{x_i}(x_i)\prod_{x_i,x_j\in\{\mathbf{x}'\},i<j}\frac{P_{x_ix_j}(x_i,x_j)}{P_{x_i}(x_i)P_{x_j}(x_j)}. \tag{4}$$

In this expression the sets $\{\mathbf{x}'\}$ and $\{x'\}$ are *any* sets of atomic sites and species (including the ''center'' atoms), but in the approximation used here, $P_{x_ix_j}(x_i,x_j)$ is only nonzero when (x_j-x_i) is a nearest- or next-nearest neighbor lattice vector.

For example, in the first- and second-neighbor pair approximation of a square lattice, if one fixes the atom types $X_1,\ldots,X_{10}$ at the sites $\mathbf{x}_1,\ldots,\mathbf{x}_{10}$ shown in Fig. 1, and computes the probability of an A-B pair at $\mathbf{r}$ and $\mathbf{r}+\delta$, then Eq. (4) yields

$$\begin{aligned}P_{AB\{x\}}(\mathbf{r},\mathbf{r}+\delta,\{\mathbf{x}\}) &= P_{AB}(\mathbf{r},\mathbf{r}+\delta)P_{X_1A}(\mathbf{x}_1,\mathbf{r})P_{AX_3}(\mathbf{r},\mathbf{x}_3)P_{BX_4}(\mathbf{r}+\delta,\mathbf{x}_4)P_{BX_6}(\mathbf{r}+\delta,\mathbf{x}_6) \\ &\times P_{X_8B}(\mathbf{x}_8,\mathbf{r}+\delta)P_{X_9A}(\mathbf{x}_9,\mathbf{r})P_{AX_2}(\mathbf{r},\mathbf{x}_2)P_{AX_4}(\mathbf{r},\mathbf{x}_4)P_{BX_3}(\mathbf{r}+\delta,\mathbf{x}_3)P_{BX_5}(\mathbf{r}+\delta,\mathbf{x}_5) \\ &\times P_{X_7B}(\mathbf{x}_7,\mathbf{r}+\delta)P_{X_8A}(\mathbf{x}_8,\mathbf{r})P_{X_9B}(\mathbf{x}_9,\mathbf{r}+\delta)P_{X_{10}A}(\mathbf{x}_{10},\mathbf{r}) \Big/ [P_A(\mathbf{r})]^7[P_B(\mathbf{r}+\delta)]^7.\end{aligned} \tag{5}$$

In Eq. (5), the correlations for the pairs that are not directly connected to the interchanging pair have been neglected as a further approximation.

There are two ways to calculate the rate constants. One was given by Vineyard,

$$R_{AB}(\{x\})=\upsilon\ \exp\left\{-\frac{U+1/2\Delta E}{k_BT}\right\}, \tag{6}$$

where U is the average activation energy for an AB exchange, and υ is the vibrational frequency associated with

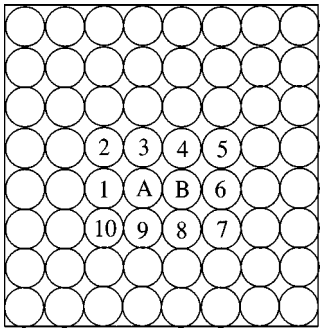

FIG. 1. Schematic illustration of the exchanging pair (A-B) and the influencing lattice sets (1–10) around the pair.

the AB exchange. ΔE depends on the types of atoms occupying the influence sites $\{x\}$. The potential energy of the system as a function of a coordinate measuring the fractional displacement of the pair from the AB configuration toward to the BA configuration is schematically shown in Fig. 2. Formula (6) is equivalent to recipe 1 described by Kikuchi in his PPM formulation.[17] Since $v\ \exp(-U/k_BT)$ occurs in all configurations, it can be combined with the time t in the kinetic equations of motion to give a dimensionless reduced time t^*,

$$t^* = t \times v\ \exp(-U/k_BT). \tag{7}$$

The rate constants can also be calculated by considering only the initial state before an atom exchange, i.e., by calculating the total-energy increase due to broken bonds during the atom exchange, or called recipe II in PPM.[17] The difference in kinetics obtained using the two methods of calculating the rate constants will be discussed later.

In a computer simulation using the set of kinetic equations (1), first one needs to construct a supercell containing a certain number of lattice sites. Then, initial values for the point and pair distribution functions are assigned at each lattice site. For example, for a completely homogeneous disordered state quenched from an infinite temperature, one may set

$$P_A(\mathbf{r}) = C_A + \zeta(\mathbf{r}). \tag{8}$$

$$P_{AA}(\mathbf{r}_1,\mathbf{r}_2) = P_A(\mathbf{r}_1)P_A(\mathbf{r}_2)\ \ \text{etc.}, \tag{9}$$

where $\zeta(\mathbf{r})$ are small random perturbations to the average composition C_A at lattice site $\mathbf{r}$. All other point and pair distribution functions are obtained from the normalization conditions given in Eq. (1). Based on the initial values for the point and pair distribution functions as well as the A-A, B-B, and A-B bond energies and temperature, the rates of change for the point and pair variables are calculated according to the right-hand sides of the kinetic equations (2) and (3). Finally, the equations are integrated using numerical integrations, e.g., the explicit Euler technique,

$$P_A(\mathbf{r},t+\Delta t) = P_A(\mathbf{r},t) + \frac{dP_A(\mathbf{r},t)}{dt} \times \Delta t,$$
$$P_{AA}(\mathbf{r}_1,\mathbf{r}_2,t+\Delta t) = P_{AA}(\mathbf{r}_1,\mathbf{r}_2,t) + \frac{dP_{AA}(\mathbf{r}_1,\mathbf{r}_2,t)}{dt} \times \Delta t, \tag{10}$$

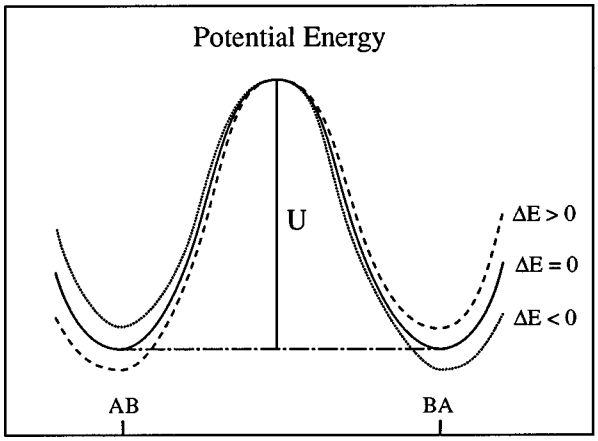

FIG. 2. Illustration of the activation energy for the A-B exchanging process with the potential energy of the system plotted as a function of a coordinate measuring the fractional displacement of the pair from the AB configuration toward to the BA configuration.

where Δt is the time step for integration. All the information about ordering and phase separation such as local composition, local long-range order, short-range order, antiphase domain, or composition domain size can be obtained from the spatial point and pair distribution functions at a given time t.

The present model has the following features: (i) with the knowledge of atom-atom bond energies and the initial distributions, the temporal evolution of point and pair distribution functions obtained from the kinetic equations automatically describes the kinetics of long-range order, short-range order, phase separation, and coarsening; (ii) in contrast to models that are linear with respect to thermodynamic driving forces, the present model is valid for large driving forces; (iii) the dependence of atomic mobility on local configuration is automatically taken into account; and (iv) at equilibrium, it produces the same equilibrium distribution functions as derived from the cluster variation method (CVM) at the same level of approximation as shown by Bakai and Fateev for bcc and fcc lattices[33] and demonstrated by the simulation results for the pair approximation discussed below.

RELATION BETWEEN ORDER PARAMETERS AND DISTRIBUTION FUNCTIONS

It is well known that long-range order is related to the point distribution function and the short-range order is related to the pair distribution functions. For a homogeneous system, it is straightforward to calculate the value of long-range order from the point distribution function. For example, for an ordered phase with two sublattices, the point distribution function has only two different values. If the two sublattices have equal number of lattice sites, such as the checkerboard order in the square lattice and $B2$ order in the bcc lattice, the two values for the point distribution function are

$$P_A^1 = C_A + C_A\eta \quad \text{and} \quad P_A^2 = C_A - C_A\eta, \tag{11}$$

where C_A is the composition of A atoms and η is the long-range order parameter. Therefore,

$$C_A = \tfrac{1}{2}(P_A^1 + P_A^2) \tag{12}$$

and

$$\eta=(P_A^1-P_A^2)/(P_A^1+P_A^2). \tag{13}$$

If a system is inhomogeneous, e.g., an ordered phase with antiphase domain boundaries or a two-phase mixture of ordered and disordered phases, the calculation of local composition and long-range order parameter from the inhomogeneous point distribution function is less obvious. Let us look at a simple example of checkerboard order in the two-dimensional square lattice. According to the concentration wave method of Khachaturyan,[34] the point distribution function for a homogeneous ordered phase can be written as

$$P_A(\mathbf{r})=C_A+C_A\eta e^{-i\mathbf{k}_o\cdot\mathbf{r}}, \tag{14}$$

where $\mathbf{k}_o$ is the superlattice vector for the ordered phase. For the checkerboard order, $\mathbf{k}_o=(2\pi/a_o)(\frac{1}{2},\frac{1}{2})$ where a_o is the lattice parameter of the square lattice. For an inhomogeneous system, both C_A and η are functions of position, i.e.,

$$P_A(\mathbf{r})=C_A(\mathbf{r})+C_A(\mathbf{r})\,\eta(\mathbf{r})e^{-i\mathbf{k}_o\cdot\mathbf{r}}. \tag{15}$$

Substituting the superlattice vector $\mathbf{k}_o$ for the checkerboard order into Eq. (15), we have

$$\begin{aligned}P_A(\mathbf{r})&=C_A(\mathbf{r})+C_A(\mathbf{r})\,\eta(\mathbf{r})e^{-i\pi(m+n)}\\&=C_A(\mathbf{r})+C_A(\mathbf{r})\,\eta(\mathbf{r})(-1)^{n+m},\end{aligned} \tag{16}$$

where m and n are integers defined in $\mathbf{r}=a_o(m,n)$. In this particular example, the local composition $C_A(\mathbf{r})$ can be approximated by

$$C_A(\mathbf{r})=\frac{1}{2z}\left[\sum_{\delta}P_A(\mathbf{r}+\delta)+P_A(\mathbf{r})\right], \tag{17}$$

where z is the number of nearest neighbors ($z=4$ for the square lattice) and δ denotes the summation over the nearest-neighbor sites of lattice point $\mathbf{r}$. Therefore, the local long-range order parameter is calculated as

$$\eta(\mathbf{r})=[P_A(\mathbf{r})-C_A(\mathbf{r})]/[C_A(\mathbf{r})(-1)^{m+n}]. \tag{18}$$

One can also define the average long-range order to characterize the degree of order of an inhomogeneous system,

$$\overline{\eta}=\frac{1}{N}\sum_{\mathbf{r}}|\eta(\mathbf{r})|, \tag{19}$$

where N is the total number of lattice sites and $|\cdots|$ denotes absolute value.

The short-range order parameter is usually defined in the disordered state in which the diffuse scattering intensity is measured experimentally. For a disordered state, $P_A(\mathbf{r})=C_A$ and the short-range order parameter is given by

$$\sigma(\mathbf{r},\mathbf{r}')=\langle[n_A(\mathbf{r})-C_A][n_A(\mathbf{r}')-C_A]\rangle/C_A(1-C_A), \tag{20}$$

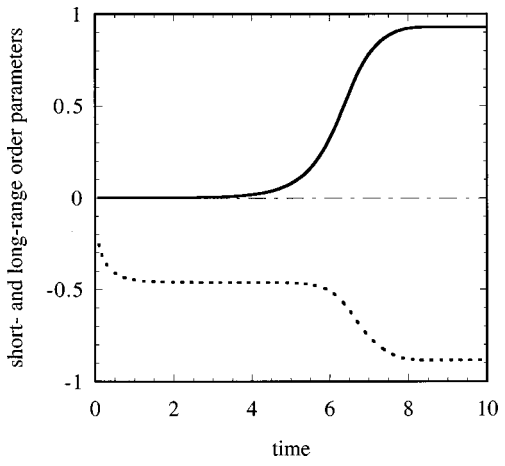

FIG. 3. Plot of short- and long-range order parameters as a function of reduced time for the case of homogeneous ordering. Solid line: long-range order parameter; dotted line: nearest-neighbor short-range order parameter.

where $\langle\cdots\rangle$ denotes ensemble averaging and $n_A(\mathbf{r})$ is defined as

$$n_A(\mathbf{r})=\begin{cases}1 & \text{if } \mathbf{r} \text{ is occupied by } A\\ 0 & \text{if } \mathbf{r} \text{ is occupied by } B.\end{cases} \tag{21}$$

From the definitions of distribution functions, one has

$$P_A(\mathbf{r})=\langle n(\mathbf{r})\rangle \quad \text{and} \quad P_{AA}(\mathbf{r},\mathbf{r}')=\langle n(\mathbf{r})n(\mathbf{r}')\rangle.$$

Therefore, in terms of pair distribution functions, we can rewrite, for a disordered state, the short-range order parameter as

$$\sigma(\mathbf{r},\mathbf{r}')=[P_{AA}(\mathbf{r},\mathbf{r}')-C_A^2]/C_A(1-C_A). \tag{22}$$

One can also use the average value of the short-range order parameter to characterize the short-range order of an inhomogeneous system. For example, for the nearest-neighbor short-range order parameter, the average value is defined as

$$\begin{aligned}\overline{\eta}&=\frac{1}{4N}\sum_{\delta}\sum_{\mathbf{r}}\sigma_{AA}(\mathbf{r},\mathbf{r}+\delta)\\&=\frac{1}{4N}\sum_{\delta}\sum_{\mathbf{r}}\frac{[P_{AA}(\mathbf{r},\mathbf{r}+\delta)-C_A^2(\mathbf{r})]}{C_A(\mathbf{r})[1-C_A(\mathbf{r})]}.\end{aligned} \tag{23}$$

RESULTS AND DISCUSSION

Kinetics of homogeneous short- and long-range order

The ordering kinetics in homogeneous systems can be easily obtained by solving kinetic equations (2) and (3), which are formulated for inhomogeneous systems, by choosing a supercell whose size is much smaller than the typical size of antiphase domains. For this purpose, we chose a 4×4 supercell with periodic boundary conditions. The bond energies were chosen in such a way that ordering of a disordered state results in the checkerboard ordered structure that has the superlattice vector of $(2\pi/a_o)(\frac{1}{2},\frac{1}{2})$. We studied the

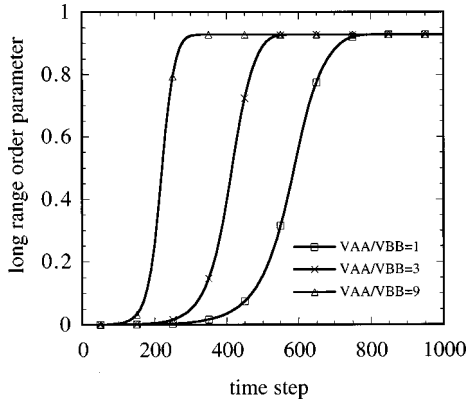

FIG. 4. Long-range order parameter as a function of reduced time for different V_{AA}/V_{BB}.

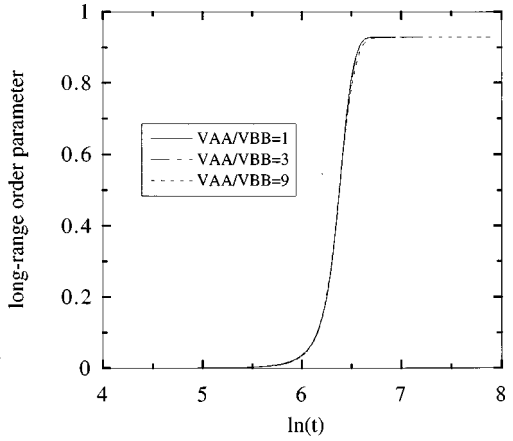

FIG. 5. Replot of Fig. 4 using ln(t) instead of t and shift the curves for $V_{AA}/V_{BB}=3$ and 9 along the ln(t) axis.

simple case of stoichiometric composition for the ordered phase, i.e., the overall average composition is chosen to be $\frac{1}{2}$. In this case we can define the long-range and short-range order parameters in terms of the point and pair distribution functions as follows:

$$\eta=|2P_A(\mathbf{r})-1| \tag{24}$$

and

$$\sigma=4\langle P_{AA}(\mathbf{r},\mathbf{r}+\delta)\rangle-1. \tag{25}$$

The relaxation kinetics of long- and short-range order for the case of the nearest-neighbor interaction model ($\varepsilon_1=V^1_{AA}+V^1_{BB}-2V^1_{AB}=1.0$ and $V^1_{AA}=V^1_{BB}$, where ε_1 is called the nearest-neighbor effective interchange energy, and V^1_{AA}, V^1_{BB}, V^1_{AB} are the nearest-neighbor A-A, B-B, and A-B bond energies, respectively) are shown in Fig. 3. The initial condition corresponds to the completely disordered state described by Eqs. (8) and (9). The time step for integration is chosen to be 0.01 in a dimensionless reduced time unit. In Fig. 3 the dotted and solid lines represent the time dependencies of the short- and long-range order parameters, respectively. Since the initial state corresponds to a completely disordered state, the initial values for both short- and long-range order parameters are zero. It is shown that the initial stage of ordering involves a very fast increase in the absolute value of the short-range order (within the first 0.4 reduced time) followed by a stationary stage in which the value of the long-range order parameter is still zero and that of the short-range order parameter is essentially a constant as a function of time. The value of long-range order starts to grow at the reduced time of about 5.0 and reaches the equilibrium value at reduced time of about 8.0. During this stage the magnitude of short-range order also increases, as shown in Fig. 3. Since the time for short-range order is substantially less than those for long-range order, it seems that the short-range order proceeds in a manner ''slaved'' to the long-range order development—which is on a longer time scale.

We checked the numerical values of the point and pair distribution functions after a system reaches equilibrium and compared it to those obtained from an equilibrium CVM calculation. In particular, we examined the following relationships obtained by minimizing a CVM free-energy functional with respect to the independent point and pair variables:[35]

$$P_{AB}P_{BA}=P_{AA}P_{BB}\exp[\varepsilon_1/k_BT] \tag{26}$$

and

$$\left(\frac{P_A(\mathbf{r}_\alpha)}{P_B(\mathbf{r}_\alpha)}\frac{P_B(\mathbf{r}_\beta)}{P_A(\mathbf{r}_\beta)}\right)^3=\left(\frac{P_{AB}(\mathbf{r}_\alpha,\mathbf{r}_\beta)}{P_{BA}(\mathbf{r}_\alpha,\mathbf{r}_\beta)}\right)^4, \tag{27}$$

where P_{AB}, P_{BA}, P_{AA}, and P_{BB} are the nearest-neighbor pair distribution functions, $\mathbf{r}_\alpha$ and $\mathbf{r}_\beta$ denote the α and β sublattices in the ordered state, and ε_1 is the nearest-neighbor effective interchange energy. After a system reaches equilibrium, both relations (26) and (27) are found to be satisfied. Therefore, the equilibrium states produced from the microscopic master equations are indeed the same as those from the equilibrium CVM technique.

Effect of relative A-A and B-B bond energies on ordering kinetics

As discussed above, the rate constants R in Eqs. (2) and (3) can be calculated in two different ways. If the rate constants are calculated using expression (6), and if we assume U is a constant, R will depend only on the effective interchange energies, not on the relative values of V_{AA} and V_{BB} bond energies. If we determine the rate constants by considering only the total energy increase due to broken bonds during the atom exchange, the ordering kinetics appear to depend on both the effective interchange energies and the relative magnitudes of V_{AA} and V_{BB}. As an illustration, the development of long-range order in the pair approximation with the same effective interchange energy but different V_{AA} to V_{BB} ratios is shown in Fig. 4. It is quite clear that the larger the ratio of V_{AA} to V_{BB}, the shorter the incubation time for ordering. When $V_{AA}/V_{BB}=1$, the kinetics obtained from the two methods of calculating R are the same. However, it should be pointed out that the differences in the incubation times for ordering may be eliminated by defining different reduced time units for different V_{AA}/V_{BB} or change

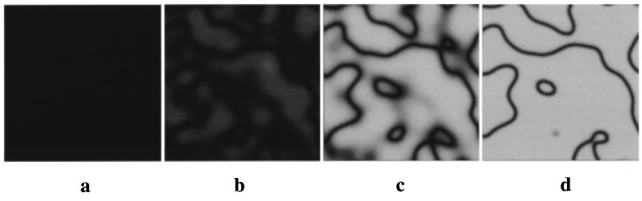

FIG. 6. Morphological pattern formation and evolution during ordering in the pair approximation. The gray levels represent the magnitude of the long-range order parameter squared. The corresponding time for each picture in the unit of reduced time is indicated in Fig. 7.

the value for U in expression (7). For example, if we replot Fig. 4 using long-range order parameter vs $\ln(t)$ instead of t and shift the curves along the $\ln(t)$ axis (Fig. 5), all the curves for different V_{AA}/V_{BB} are shown to superimpose on each other.

Morphological pattern formation during ordering

Since the kinetic equations are written for inhomogeneous systems, the temporal morphological patterns during ordering are automatically described by the time-dependent spatial distribution of order-parameter profiles that can be determined from the inhomogeneous point distribution functions as shown in Eq. (18). The temporal evolution of the spatial long-range order during an order-disorder transformation is shown in Fig. 6 for a computational cell of 128×128 lattice sites with periodic boundary conditions. The corresponding plot of the average long-range order parameter as a function of reduced time is shown in Fig. 7. A nearest-neighbor interaction model ($\varepsilon_1=1.0$ and $V^1_{AA}=V^1_{BB}$) in the pair approximation was employed. The initial condition corresponds to the disordered state with small random perturbations. The time step for integration is 0.01 in a dimensionless reduced time unit. The temperature for the simulation is $0.5\varepsilon_1/k_B$ where k_B is the Boltzmann constant. The different gray levels in Fig. 6 represent the values of η^2, where η is the long-range order parameter. Bright regions are ordered domains with η^2 close to 1.0 and dark regions are the disordered phase with η^2 near 0.0. Therefore, the dark lines in

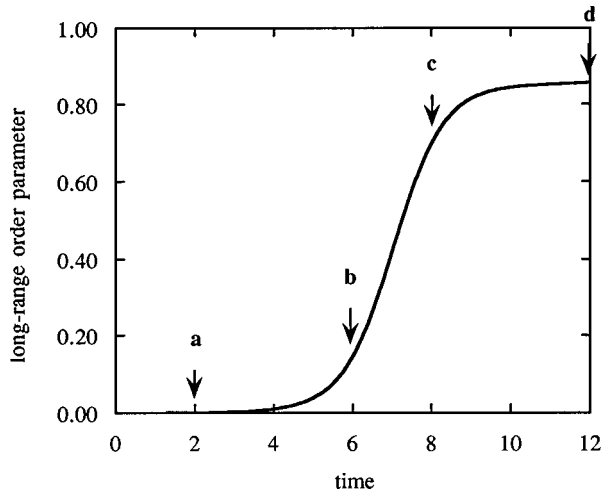

FIG. 7. The average long-range order parameter as a function of time for ordering in an inhomogeneous system.

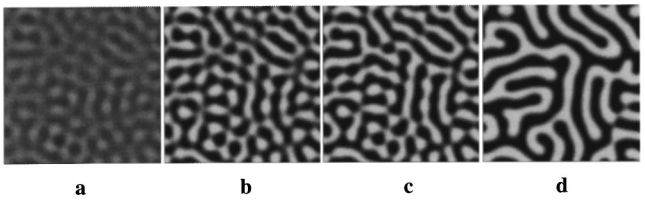

FIG. 8. Morphological pattern formation and evolution during spinodal decomposition in the pair approximation. The gray levels represent the magnitude of the absolute value of the local composition deviation from the overall composition. The corresponding time for each picture in the unit of reduced time is indicated in Fig. 9.

Fig. 6 are antiphase domain boundaries. The time and the average value of the long-range order parameter corresponding to each picture in Fig. 6 are indicated in Fig. 7. Figure 6(a), corresponding to point a in Fig. 7, is still a disordered state where values of η^2 at each lattice site are near zero. Figure 6(b) shows the initial growth of ordered domains with an average value of the long-range order parameter around 0.20. The average value of the long-range order parameter reaches near the equilibrium value at a time equal to about 8.0 in the reduced unit and the corresponding domain morphology is shown in Fig. 6(c). Figures. 6(c) and 6(d) display the antiphase domain coarsening process. It may be noticed that the time dependencies of the long-range order parameter are almost the same for a homogeneous system (Fig. 3) and an inhomogeneous system (Fig. 7).

Morphological pattern formation during spinodal decomposition

The morphological evolution during a spinodal decomposition in the pair approximation and a nearest-neighbor interaction model ($\varepsilon_1=-1.0$) is shown in Fig. 8 in which the gray levels represent the magnitudes of local composition. The overall average composition is 0.5. A computational cell of 128×128 lattice sites with periodic boundary conditions was employed. The initial condition corresponds to a homogeneous solution with small random perturbations. The time step for integration is 0.1 in a dimensionless reduced time unit. The temperature for the simulation is $-0.5\varepsilon_1/k_B$. The average composition wave amplitude ($|C(r)-C_o|$ where $C(r)$ is the local composition and C_o is the overall average composition) as a function of time during spinodal decomposition is plotted in Fig. 9. The correspondence between Figs. 8 and 9 are labeled in Fig. 9.

Comparison between point and pair approximations

The kinetics of long-range order obtained from the pair approximation and the point approximation are compared in Fig. 10 with the same simulation temperature and system size. The most significant difference is the fact that the incubation time in the pair approximation (solid line) is much longer than that in the point approximation (dotted line). It may also be noticed that the time for the long-range order to reach the equilibrium value from the initial growth is longer in the pair approximation ($t^*=5.0-8.0$) than that in the point approximation ($t^*=1.0-2.0$), and that the incubation time also depends on the initial conditions, e.g., the ampli-

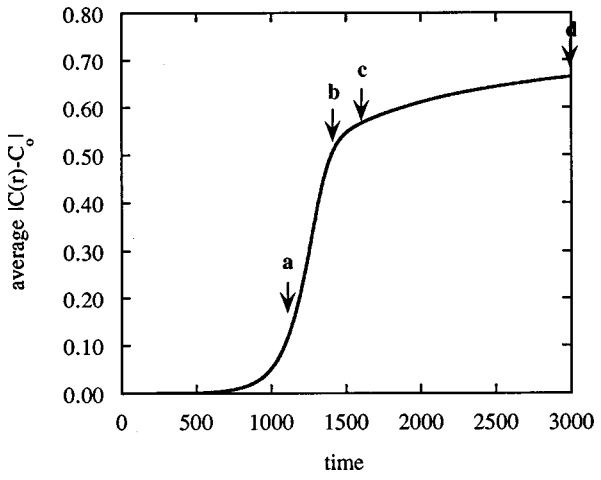

FIG. 9. The average absolute value of the local composition deviation from the overall composition as a function of time for the case of spinodal decomposition and pair approximation in an inhomogeneous system.

tudes of random fluctuations introduced into the initial point and pair distribution functions.

We also compared morphological evolution in the point and pair approximations. The morphological evolution for the point approximation in Fig. 11 was obtained using exactly the same initial condition as in the pair approximation and the corresponding plot of average long-range order parameter against time is shown in Fig. 10 as the dotted line. A comparison of Figs. 6(c) and 11(b) indicates that although the domain morphologies look similar in two approximations, the average domain size in the pair approximation is larger than that in the point approximation for the time at which the ordering is near completion.

The difference between the point and pair approximations is much more striking in the case of spinodal decomposition than in the case of ordering. The morphological evolution for the point approximation is shown in Fig. 12. The corresponding plot of average deviation of composition from the overall composition is shown in Fig. 13. First of all, it may be noticed that there are more than two orders of magnitude difference in the incubation times between the pair approximation and the point approximation, i.e., the time period before any significant growth of composition wave amplitude occurs (compare Figs. 9 and 13). Second, the morphology after decomposition and before any significant coarsening shows much coarser scale in the case of pair approximation than that in the point approximation, even though the morphologies in the two cases are very similar except in the scale.

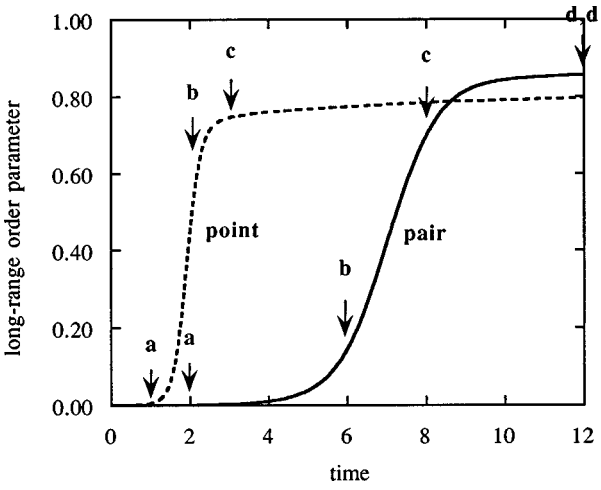

FIG. 10. The variation of long-range order parameter as a function of time for the case of point approximation (dotted line) and the case of pair approximation (solid line).

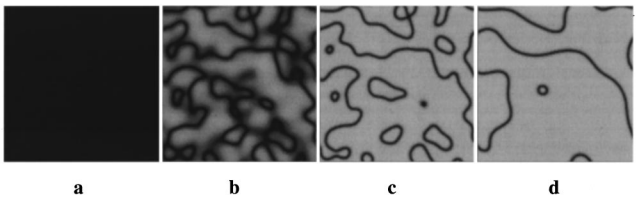

FIG. 11. Morphological pattern formation and evolution during ordering in the point approximation. The gray levels represent the magnitude of the long-range order parameter squared. The corresponding time for each picture in the unit of reduced time is indicated in Fig. 10 on the dotted line.

To give a simple explanation for the difference in kinetics between point and pair approximations, i.e., the effect of pair correlation on the ordering and phase separation kinetics, we define the following free energy in the pair approximation and a nearest-neighbor interaction model

$$F=\frac{1}{2}\sum_{r_1-r_2=\delta}\sum_{\alpha}\sum_{\beta}V_{\alpha\beta}(r_1,r_2)P_{\alpha\beta}(r_1,r_2)$$
$$-k_BT\Bigg[(z-1)\sum_{r}\sum_{\alpha}P_{\alpha}(r)\ln P_{\alpha}(r)$$
$$-\frac{1}{2}\sum_{r_1-r_2=\delta}\sum_{\alpha}\sum_{\beta}P_{\alpha\beta}(r_1,r_2)\ln[P_{\alpha\beta}(r_1,r_2)]\Bigg], \tag{28}$$

where r, r_1, r_2 represent lattice positions, δ nearest-neighbor distance, α and β atom species, z the number of nearest neighbors, $V_{\alpha\beta}$ the bond energies as discussed above, and $P_{\alpha\beta}$ pair probabilities. Using this definition, the nonequilibrium free energies as a function of time in the point and pair

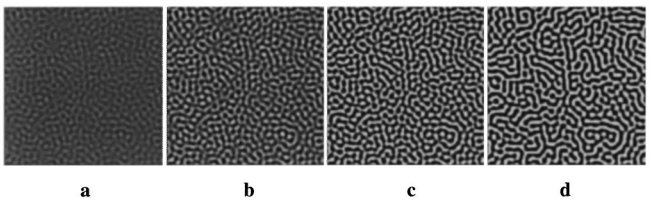

FIG. 12. Morphological pattern formation and evolution during spinodal decomposition in the point approximation. The gray levels represent the magnitude of the absolute value of the local composition deviation from the overall composition. The corresponding time for each picture in the unit of reduced time is indicated in Fig. 13.

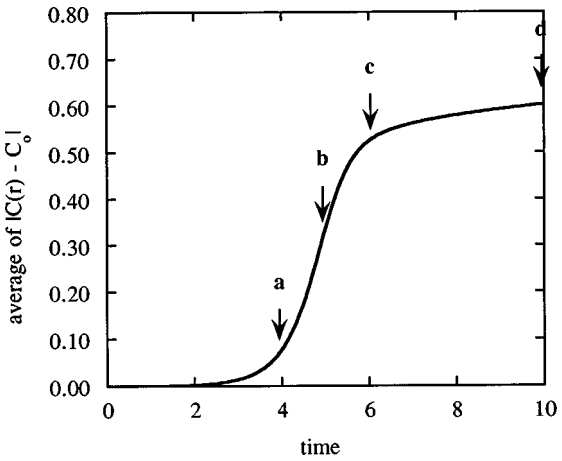

FIG. 13. The average absolute value of the local composition deviation from the overall composition as a function of time for the case of spinodal decomposition and point approximation in an inhomogeneous system.

approximations are plotted in Fig. 14 for the case of ordering. It is shown that the short-range order relaxation results in a significant drop in the total free energy (more than half the total free energy decreases from the initially completely disordered state to the equilibrium ordered state). As a result, the driving force for the development of long-range order is significantly reduced, resulting in a much longer incubation time in the pair approximation. Similar to the case of ordering, the difference in the kinetics between the point and pair approximations for spinodal decomposition is also due to the difference in the driving forces. However, the effect of the driving force on the incubation time is more dramatic in the case of spinodal decomposition than ordering.

Kinetics of long-range order with slaved short-range order

As demonstrated above, the kinetics of short-range order relaxation is much faster than the development of long-range order or compositional inhomogeneities. As a result, at a given state of long-range order or compositional distribution, the system is essentially at equilibrium with respect to the

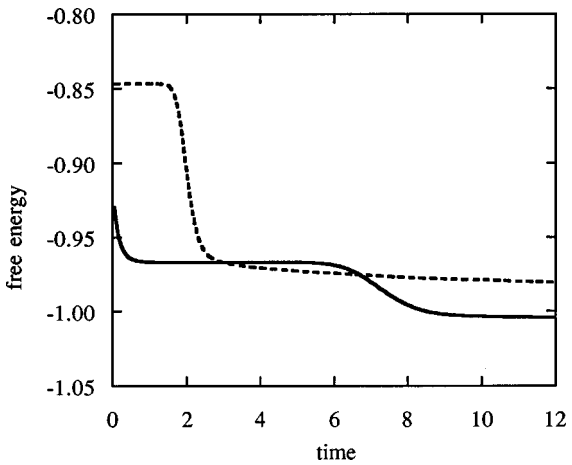

FIG. 14. Free energy as a function of time for the case of ordering in the point approximation (dotted line) and the pair approximation (solid line) in an inhomogeneous system.

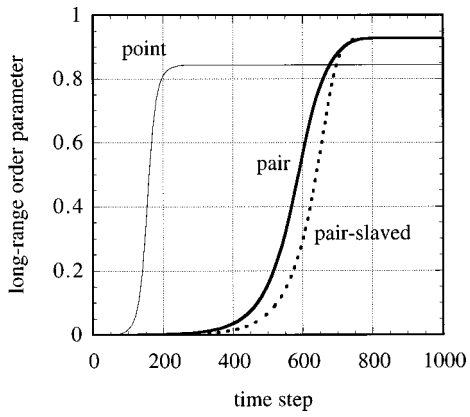

FIG. 15. Long-range order parameter obtained by assuming instantaneous equilibrium with respect to short-range order (pair slaved), the pair approximation (pair), and the point approximation (point).

short-range order. Therefore, one may describe the kinetics of long-range order or compositional spinodal decomposition by assuming instantaneous establishment of equilibrium with respect to short-range order, i.e., the pair correlations only affect the thermodynamic driving force. Figure 15 shows the kinetics of long-range order obtained by first minimizing the CVM free energy with respect to the pair variables, then expressing these pair variables in terms of point variables, and only solving the kinetic equations for the point variables. Also included in Fig. 15 is the time dependence of average long-range order parameter obtained in the pair approximation. Although there are differences in the kinetics obtained from the true pair approximation and that with slaved pair correlations, the difference is quite small compared to the difference between the true pair approximation and point approximation as shown in Fig. 10. It is expected that higher-order correlation functions also relax much faster than point distribution functions that characterize the long-range order or compositional distribution. In principle, one can approximate the kinetics of long-range order and phase separation by assuming that all the correlation functions are instantaneously established. Therefore, one could express the correlation functions in terms of point variables by minimizing the corresponding CVM free energy with respect to all high-order correlation functions, and only the kinetic equations for the point variables needs to be solved for effectively taking into account high-order correlations on the kinetics.

SUMMARY

We have developed a computer simulation technique based on microscopic master equations in the pair approximation for studying the kinetics of atomic ordering and phase separation in highly nonequilibrium and inhomogeneous systems. We showed that for a homogenous system at completely thermodynamic equilibrium, the kinetic equations produce the same equilibrium states as the CVM of equilibrium statistical thermodynamics. We observed quite different ordering and phase separation kinetics between the single-site point approximation and the pair approximation. It is shown that the development of long-range order and growth of concentration waves are significantly delayed due

to their coupling to the relaxation of short-range order in the pair approximation as compared to those obtained from the point approximation with the same initial conditions. We also showed that the kinetics of long-range order and compositional phase separation can be very well approximated by assuming that the short-range order is instantaneously established, i.e., the short-range order is slaved by the long-range order.

ACKNOWLEDGMENTS

This work was supported by the Office of Naval Research under Grant No. N00014-95-1-0577, the NSF under Grant No. DMR-96-33719, and through the ARPA/NIST program on mathematical modeling of microstructure evolution in advanced alloys. The computing time was provided by a grant from the DOD High Performance Computing Systems.

[1] J. W. Cahn, Acta Metall. **9**, 795 (1961).
[2] S. M. Allen and J. W. Cahn, Acta Metall. **27**, 1085 (1979).
[3] A. G. Khachaturyan, Fiz. Tverd. Tela **9**, 2595 (1967) [Sov. Phys. Solid State **9**, 2040 (1968)].
[4] L. Q. Chen, Mod. Phys. Lett. B **7**, 1857 (1993), and references therein.
[5] Y. Z. Wang, L. Q. Chen, and A. G. Khachaturyan, in *Computer Simulation in Materials Science-Nano/Meso/Macroscopic Space and Time Scales* Vol. 308 of *NATO Advanced Study Institute Series E: Physics*, edited by H. O. Kirchner, K. P. Kubin, and V. Pontikis (Kluwer-Academic, New York, 1996), pp. 325–371 and references therein.
[6] L. Q. Chen and Y. Z. Wang, JOM **48**, 13 (1996), and references therein.
[7] G. H. Vineyard, Phys. Rev. **102**, 981 (1956).
[8] C. M. van Baal, Physica A **111**, 591 (1982).
[9] C. M. van Baal, Physica A **113**, 117 (1982).
[10] C. M. van Baal, Physica A **129**, 601 (1985).
[11] B. Fultz, Acta Metall. **37**, 823 (1989).
[12] B. Fultz, J. Mater. Res. **5**, 1419 (1990).
[13] G. Martin, Phys. Rev. B **41**, 2279 (1990).
[14] J.-F. Gouyet, Europhys. Lett. **21**, 335 (1993).
[15] O. Penrose, J. Stat. Phys. **63**, 975 (1991).
[16] R. Kikuchi, Ann. Phys. (Leipzig) **10**, 127 (1960).
[17] R. Kikuchi, Prog. Theor. Phys. Suppl. **35**, 1 (1969).
[18] K. Gschwend, H. Sato, and R. Kikuchi, J. Phys. (Paris), Colloq. **38**, C7-357 (1977).
[19] K. Gschwend, H. Sato, and R. Kikuchi, J. Chem. Phys. **69**, 5006 (1978).
[20] K. Gschwend, H. Sato, and R. Kikuchi, J. Chem. Phys. **71**, 2844 (1979).
[21] H. Sato and R. Kikuchi, Acta Metall. **24**, 797 (1976).
[22] T. Mohri, in *Solid-Solid Phase Transformations*, edited by W. C. Johnson, J. M. Howe, D. E. Laughlin, and W. A. Soffa (The Minerals, Metals & Materials Society, Warrendale, PA, 1994), p. 53.
[23] C. M. van Baal, Physica A **196**, 116 (1993).
[24] L. Q. Chen and J. A. Simmons, Acta Metall. Mater. **42**, 2943 (1994).
[25] L. Q. Chen, in *Defect Interface Interactions*, MRS Symposia Proceedings No. 319, edited by E. P. Kvam, A. H. King, M. J. Mills, T. D. Sands, and V. Vitek (Materials Research Society, Pittsburgh, 1994), p. 375.
[26] C. W. Geng and L. Q. Chen, Scr. Metall. Mater. **31**, 1507 (1994).
[27] C. W. Geng and L. Q. Chen, Surf. Sci. **355**, 229 (1994).
[28] V. G. Vaks, S. V. Beiden, and V. Yu. Dobretsov, Pis'ma Zh. Eksp. Teor. Fiz. **61**, 65 (1995) [JETP Lett. **61**, 68 (1995)].
[29] V. Yu. Dobretsov, G. Martin, F. Soisson, and V. G. Vaks, Europhys. Lett. **31**, 417 (1995).
[30] V. Yu. Dobretsov, V. G. Vaks, and G. Martin, Phys. Rev. B **54**, 3227 (1996).
[31] M. Plapp and J.-F. Gouyet, Phys. Rev. Lett. **78**, 4970 (1997).
[32] M. Plapp and J.-F. Gouyet, Phys. Rev. E **55**, 45 (1997).
[33] A. S. Bakai and M. P. Fateev, Phys. Status Solidi B **158**, 81 (1990).
[34] A. G. Khachaturyan, *Theory of Structural Transformations in Solids* (Wiley, New York, 1983).
[35] R. Kikuchi (unpublished).